SiF 2024 – The 13th International Conference on Structures in Fire
University of Coimbra, Portugal, 19 to 21 June 2024

RESISTANCE MODELS FOR THIN-WALLED STEEL BEAMS UNDER NON-UNIFORM TEMPERATURE USING MACHINE LEARNING

Carlos Couto[1], Qi Tong[2], Thomas Gernay[3]

ABSTRACT

The resistance of thin-walled steel beams in fire is governed by a complex interaction between the buckling of the plates and the lateral-torsional buckling (LTB) of the member, combined with the temperature-induced reduction of steel properties. Besides, in many applications, steel beams are subjected to non-uniform thermal exposure which creates temperature gradients in the section. There is a lack of analytical design methods to capture the effects of temperature gradients on the structural response, which leads to overly conservative assumptions thwarting optimization efforts. Meanwhile, data-based Machine Learning (ML) methods have been widely recognized for their ability to learn from complex dataset and generate predictive models. This paper describes the development of four different ML models for thin-walled steel beams subjected to thermal gradients. A parametric heat transfer analysis is first conducted to characterize the thermal gradients that develop under three-sided fire exposure. Nonlinear finite element simulations with shells are then used to generate the resistance dataset. The ML models, trained using physically defined features, show significant improvement in predictive capacity over the Eurocode methods. The ML-based models can be used to improve existing design methods for non-uniform temperature distributions.

Keywords: Machine learning; Thin-walled beams; Fire; Temperature gradient; Shell finite elements

1 INTRODUCTION

This paper investigates opportunities from application of ML methods to the problem of thin-walled steel beams in fire subjected to non-uniform temperature gradients. Recently, ML models have been successfully developed for thin-walled members [1–3], but the effect of thermal-gradients has not been yet accounted for. While the development of ML models requires sophisticated modelling and large datasets, which may not be always available, once a ML model is developed its application to practical design situations within the limits of its validity is straightforward.

Existing analytical methods have undeniable advantages, such as confidence from accrued experience and link to physical key parameters, which allow calibration for target reliability and interpretability ("white-box") for generic applicability. Yet analytical methods have failed so far to solve some complex issues in fire, including those arising from the effects of temperature gradient. In particular, there are few studies devoted to investigation of the effect of non-uniform temperature gradients in beams [4–7]. In addition, the inclusion of novel developments into design standards is a lengthy process, for example the present version of Eurocode 3 Part 1-2 was issued in 2005 [8]. For these reasons, innovations are held back as there is no

[1] Assistant Researcher, RISCO, Civil Engineering Department, University of Aveiro, Portugal
e-mail: ccouto@ua.pt, ORCID: https://orcid.org/0000-0003-0865-2225
[2] Department of Civil and Systems Engineering, Johns Hopkins University, Baltimore, USA
e-mail: qtong5@jhu.edu
[3] Assistant Professor, Department of Civil and Systems Engineering, Johns Hopkins University, Baltimore, USA
e-mail: tgernay@jhu.edu, ORCID: https://orcid.org/0000-0002-3511-9226

legal basis for practitioners to apply recent methods with a negative impact on the industry. This motivates exploration of ML methods.

The approach in this study starts by deriving a comprehensive dataset where the samples were obtained from parametric analysis using nonlinear Finite Element (FE) with shell elements and capture the different structural failure modes (local buckling and LTB). The FE model includes non-uniform temperature distributions resulting from thermal gradients, based on an assessment of the temperature distributions in the flanges and webs occurring from three-side thermal exposure of protected beams. Then, ML-based models are derived for predicting the capacity of these thin-walled steel members at elevated temperature. The ML models include artificial neural networks (ANN), support vector regression (SVR), random forests (RF) and polynomial regression (PR). An overview of the existing analytical design rules in the Eurocode 3 Part 1-2 [8], and improved proposals [9], for predicting the capacity of these members at elevated temperature is provided with discussion of the input parameters (or features). Given that these analytical methods are based on a uniform temperature distribution in the section, the effect of different assumptions regarding their applicability to non-uniform temperature distributions is also discussed.

2 CURRENT ANALYTICAL MODELS FOR THIN-WALLED BEAMS IN FIRE

2.1 Effective cross-section

For beams with thin-walled sections, the evaluation of load carry capacity at elevated temperature must consider the effect of local buckling. Part 1.5 of Eurocode 3 provides expressions of reduction factors for plate buckling resistance under compression, based on the concept of effective width method accounting for geometric imperfection and residual stresses [10]. Couto et al. [11] proposed an updated formula to account for the local buckling of slender steel members (Class 3 and Class 4) at elevated temperature and replaced the use of design yield strength corresponding to the 0.2% proof strength with the yield strength at 2% total strain for Class 4.

The effective width of plates at elevated temperature can be calculated as:

$$b_{eff} = \rho_\theta \times b \tag{1}$$

The new expression [11] for a plate reduction factor of internal compression elements (e.g., web) is:

$$\rho_\theta = \frac{\left(\overline{\lambda}_p + \alpha_\theta\right)^{\beta_\theta} - 0.055(3+\psi)}{\left(\overline{\lambda}_p + \alpha_\theta\right)^{2\beta_\theta}} \leq 1.0 \tag{2}$$

For outstand compression elements (e.g., flanges) it is:

$$\rho_\theta = \frac{\left(\overline{\lambda}_p + \alpha_\theta\right)^{\beta_\theta} - 0.188}{\left(\overline{\lambda}_p + \alpha_\theta\right)^{2\beta_\theta}} \leq 1.0 \tag{3}$$

$\overline{\lambda}_p$ is the non-dimensional slenderness of a plate given by:

$$\overline{\lambda}_p = \frac{b/t}{28.4\varepsilon\sqrt{k_\sigma}} \tag{4}$$

where k_σ is the buckling coefficient of plates, b and t are the width and thickness of the plates, ψ is the stress ratio between two ends. Coefficients α_θ and β_θ are given in Table 2 in the reference [11] for internal compression elements and outstand compression elements. ε is calculated as:

$$\varepsilon = \sqrt{\frac{235}{f_y}}\sqrt{\frac{E}{210000}} \text{ in which } f_y \text{ and } E \text{ in Mpa} \tag{5}$$

According to the current Eurocode 3 Part 1-2 [8], the effective section is calculated for $\alpha_\theta = 0$ and $\beta_\theta = 1$.

2.2 Lateral-torsional buckling

Once the effective width of the plates is calculated and the effective properties of the section determined, the load-carrying capacity of the beam is evaluated by making allowance for lateral-torsional buckling using equation (6) according to Part 1-2 of Eurocode 3 [8].

$$M_{\mathrm{b,fi,t,Rd}} = \chi_{\mathrm{LT,fi}} \cdot M_{fi,Rd}/\gamma_{\mathrm{M,fi}} = \chi_{\mathrm{LT,fi}} \cdot W_{\mathrm{eff}} \cdot k_{\theta} \cdot f_{\mathrm{y}}/\gamma_{\mathrm{M,fi}} \tag{6}$$

where W_{eff} is the effective section modulus calculated using the effective width of the plates, k_{θ} is the reduction factor for the yield strength at elevated temperatures, f_{y} is the yield strength, $\gamma_{\mathrm{M,fi}}$ is the safety factor taken as 1.0. According to the present version of the Eurocode 3 Part 1-2, for Class 4 sections, k_{θ} is taken as the reduction factor for the 0.2% proof strength of steel at elevated temperatures ($k_{\mathrm{p,0.2,\theta}}$).

The lateral-torsional buckling reduction factor for flexural buckling $\chi_{LT,fi}$ is calculated as:

$$\chi_{LT,fi} = \frac{1}{\phi_{LT,\theta} + \sqrt{\phi_{LT,\theta}^2 - \bar{\lambda}_{LT,\theta}^2}} \quad \text{and} \quad \chi_{LT,fi} \leq 1.0 \tag{7}$$

$\bar{\lambda}_{LT,\theta}$ is the non-dimensional slenderness at elevated temperature and $\phi_{LT,\theta}$ is calculated as:

$$\phi_{LT,\theta} = 0.5\left[1 + \alpha_{LT}\bar{\lambda}_{LT,\theta} + \bar{\lambda}_{LT,\theta}^2\right] \tag{8}$$

and α_{LT} is the imperfection factor calculated as $\alpha_{LT} = 0.65\varepsilon = 0.65\sqrt{235/f_y}$. The non-dimensional slenderness at elevated temperature $\bar{\lambda}_{\theta}$ is calculated as:

$$\bar{\lambda}_{LT,\theta} = \sqrt{\frac{W_{\mathrm{eff}} \cdot k_{\theta} \cdot \frac{f_{\mathrm{y}}}{\gamma_{M,fi}}}{k_{E,\theta} M_{cr,20}}} \tag{9}$$

where $k_{E,\theta}$ is the reduction factor for Young's modulus at elevated temperatures, and $M_{cr,20}$ is the elastic critical capacity at ambient temperature which is based on the full section.

2.3 New generation of Eurocode 3 Part 1-2

In the new generation of Eurocode 3 Part 1-2 (EN 1993-1-2 New Generation) [9], the overall capacity of laterally unrestrained beams with slender cross-sections is calculated following the same procedure presented in the previous section, except that the reduction factor $\chi_{LT,fi}$ calculated using equation (7) is determined by replacing $\phi_{LT,\theta}$ in equation (8) with the $\phi_{LT,\theta,\mathrm{NG}}$ calculated according to equation (11),

$$\phi_{LT,\theta,\mathrm{NG}} = 0.5\left[1 + \alpha_{LT,\mathrm{NG}}\left(\bar{\lambda}_{LT,\theta} - 0.2\right) + \bar{\lambda}_{LT,\theta}^2\right] \tag{10}$$

where the values of the imperfection factor $\alpha_{LT,\mathrm{NG}}$ depend on the limits of the Effective Section Factor (ESF), defining three different LTB design curves named L1, L2 and L3. The ESF is the ratio between the effective modulus ($W_{\mathrm{eff},y}$) and the elastic modulus ($W_{\mathrm{el},y}$) of the cross-section and captures the role of the local buckling on the lateral-torsional buckling resistance of the beams at elevated temperature [12]. The $\alpha_{LT,\mathrm{NG}}$ is 1.25ε, 1.0ε and 0.75ε, according to the limits, $\frac{W_{\mathrm{eff},y}}{W_{\mathrm{el},y}} > 0.9$, $0.8 < \frac{W_{\mathrm{eff},y}}{W_{\mathrm{el},y}} \leq 0.9$ and $\frac{W_{\mathrm{eff},y}}{W_{\mathrm{el},y}} \leq 0.8$, respectively, defining the curves L1, L2 and L3.

The model discussed here does not incorporate the effect of non-uniform temperatures. The Eurocode 3 Part 1-2 specifies that (clause 4.2.3.4(3)) conservatively, the temperature θ in Eq. (6) can be assumed to be equal to the maximum temperature. Further discussion on this aspect is provided in Section 6.

3 ANALYSIS OF NON-UNIFORM TEMPERATURE DISTRIBUTION IN THE SECTIONS

In many applications, steel beams will be subjected to non-uniform thermal exposure resulting in temperature gradients in the section. Here, heat transfer analyses with the finite element method (FEM) is used to analyze the temperature distribution in steel cross-sections heated by the ISO 834 fire on three sides.

The fourth side of the steel profile is either in contact with a concrete slab, or with air at ambient temperature. The parametric thermal analyses are conducted in SAFIR [13] considering a range of section dimensions, insulation thickness, and the presence of the slab. The insulation is a sprayed material with a conductivity of 0.4 W/mK, specific heat of 900 J/kgK, specific mass of 40 kg/m^3, water content of 1 kg/m^3, and emissivity of 0.8. Figure 1 shows the temperature distribution in two steel profiles protected with 12.7 mm of insulation after 30 minutes of exposure to the ISO 834 fire. The analyses determine the temperature evolution in each node of the section, which is then averaged into one (transient) temperature for each plate of the cross-section. The non-uniform temperature distribution is then defined through 2 parameters: (i) the temperature of the lower flange exposed to the fire, $\theta_{fl,hot}$, and (ii) the temperature of the unexposed upper flange, $\theta_{fl,cold}$. The temperature of the web, θ_{web}, is also examined and is related to the flange temperatures. The study aims at evaluating the difference in the average temperatures between the flanges, $\theta_{fl,hot} - \theta_{fl,cold}$.

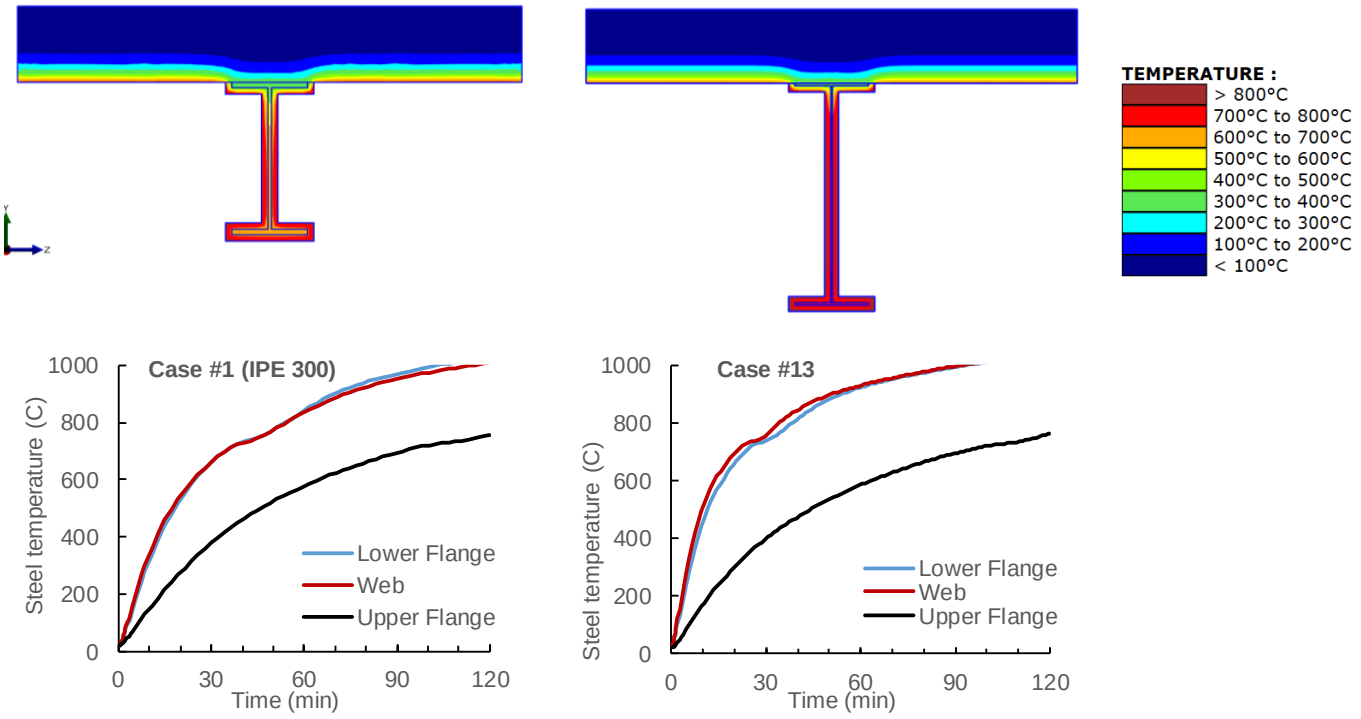

(a) IPE 300 (b) Section 450×3.2+150×5

Figure 1. Temperature distribution in protected steel beams subjected to ISO 834 fire exposure on three sides.

A sample of results are plotted in Figure 2. This plot shows, for fourteen cases, the average temperature in each of the plate after 30 min and 60 min of exposure, respectively. Cases 7 to 12 do not have a slab. It is found that the temperature of the web (θ_{web}) is consistently very close to the temperature of the lower flange ($\theta_{fl,hot}$). The θ_{web} will thus be assumed as the same as $\theta_{fl,hot}$. The difference between the flange temperatures increases when a concrete slab is present. The difference is also larger for the thin-walled section than for compact hot-rolled sections. A reasonable estimate of the temperature gradient between the flanges is found as $\theta_{fl,hot} - \theta_{fl,cold} = 150\ °C$ for profiles without slab and $\theta_{fl,hot} - \theta_{fl,cold} = 250\ °C$ for profiles with a concrete slab. Based on these analyses, four temperature distribution cases will be considered for constructing the numerical database for elevated temperature resistance of the steel beams, namely ($\theta_{fl,hot}$; $\theta_{fl,cold}$) equal to ($650\ °C; 500\ °C$), ($650\ °C; 400\ °C$), ($550\ °C; 400\ °C$), ($550\ °C; 300\ °C$).

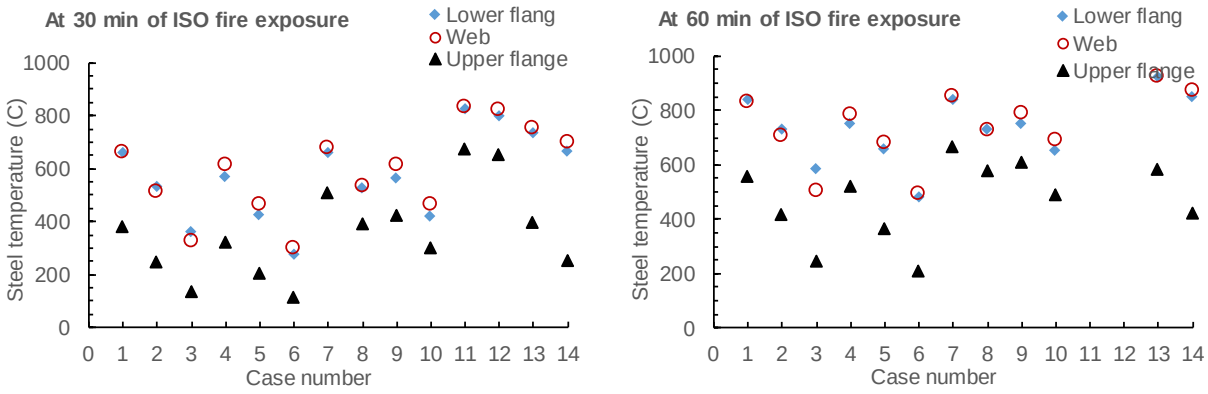

Figure 2. Calculated temperature distributions at different times of ISO fire exposure.

4 NUMERICAL MODEL AND DATASET

4.1 Finite element model

Numerical modelling was used to analyse beams made of I-shaped slender cross-sections subjected to major-axis bending at elevated temperatures. The numerical models were built using shell elements in the nonlinear finite element software SAFIR [13]. Beams with different plate slenderness, lengths and non-uniform thermal gradients were modelled. A sensitivity analysis on the mesh size was conducted to have a sufficiently refined mesh while preserving an appropriate computational cost.

The constitutive model included in the simulations followed the non-linear stress-strain relationship and reduction factors defined in Eurocode 3 Part 1-2 [8]. Steels with grades S235 and S355, corresponding to yield strength of 235 and 355 MPa at ambient temperature were used in the numerical models. Young's modulus of elasticity at ambient temperature was taken as 210 GPa and Poisson's ratio as 0.30.

Both geometric imperfections (global and local) and material imperfections, in the form of residual stresses, were included in the models. For global imperfection, the amplitude followed the design recommendation, i.e. $L/1000$, where L is the length of the member. For local imperfection, the amplitude was calculated as 80% of the geometric fabrication tolerances [14]. The global imperfection and local imperfection were combined following the recommendation of Annex C in Part 1-5 of Eurocode 3 [10]. In accordance with the recommendations of this Annex, the full amplitude was considered for the leading imperfection while that of the accompanying imperfections was reduced to 70%. The shape of these imperfections was obtained from a linear buckling analysis (LBA), using Ansys [15], following the same modelling assumptions as described here. For the residual stresses, the pattern for welded beams [14] was included in the models.

Fork-supports were used at both ends of the structural member to prevent the displacements in y-direction and z-direction. To prevent rigid body movement, the displacements in x-direction were constrained at mid-span. The loading was applied by nodal forces to produce end-moments at both ends. Additionally, a layer of thicker elements was included at the extremities to ensure correct load distribution (see Figure 3) as done in [16].

The ultimate load-bearing capacity of the beams was calculated with SAFIR considering steady-state conditions i.e., by first uniformly increasing the temperature in the section up to the target value and then progressively loading the members until failure was reached.

An example of the collapse shape of a slender beam with 450×3.2+150×5 and the corresponding boundary conditions are provided in Figure 3. More details about the numerical model can be found in [14,16].

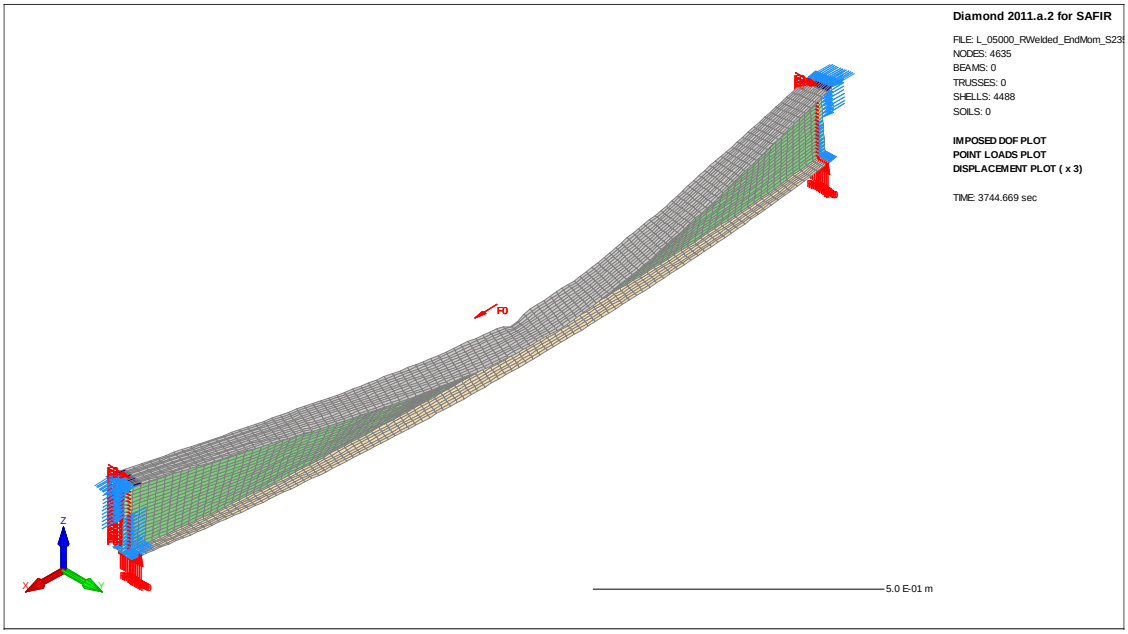

Figure 3. Collapse shape of beam 450×3.2+150×5 (S235) with L=5.0 m, $\theta_{fl,cold} = 300℃$ and $\theta_{fl,hot} = 550℃$.

4.2 Dataset

A dataset was defined where the data points were calculated using the numerical model described in the previous section. FE simulations were run to failure. The dataset includes 6348 FE simulations.

The selection of features was carried out using a procedure that combined prior knowledge about the parameters potentially influencing the mechanical response (mechanistic-informed) and a quantitative trial-and-error approach to find the most suitable combination of features. The process of feature selection dealt with both inclusion and exclusion of parameters and their combination, and the best model was selected as the one with fewest parameters for a given accuracy. The ranges of values for the input parameters are listed in Table 1, defining 8 features for the ML models.

Table 1. Input parameters/features of dataset used for the ML models training.

Notation	Feature	Input values	Min.	Max.
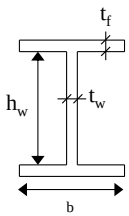	x_1	h_w/t_w	75	200
	x_2	b/t_f	9	37.5
	x_3	h_w/b	1	6.67
	x_4	t_w/t_f	0.08	1.6
	x_5	f_y/E	$(235/E)$	$(355/E)$
	x_6	$\theta_{fl,cold}$	300℃	500℃
	x_7	$\theta_{fl,hot}$	550℃	650℃
	x_8	$\left(M_{pl,20}/M_{cr,20}\right)^{0.5}$	0.16	8.25

In this table, the h_w/t_w and b/t_f are the adimensional web and flange dimensions, f_y/E is the adimensional yield strength for beams. $M_{pl,20}$ is the section plastic capacity, $M_{cr,20}$ is the elastic critical load at ambient temperature. The range of feature values considered in the dataset was chosen to cover a common range of design parameters for slender section steel beams in building structures.

The output was defined as $y = M_{\text{ult,fi}}/M_{pl,20}$ with $M_{\text{ult,fi}}$ being the ultimate capacity of a beam. The frequency distribution for each feature is plotted in Figure 4.

The 6348 samples were randomly divided on a proportion of 9:1 to create the training and testing subsets, thus 5713 cases were considered for training and 635 cases for testing.

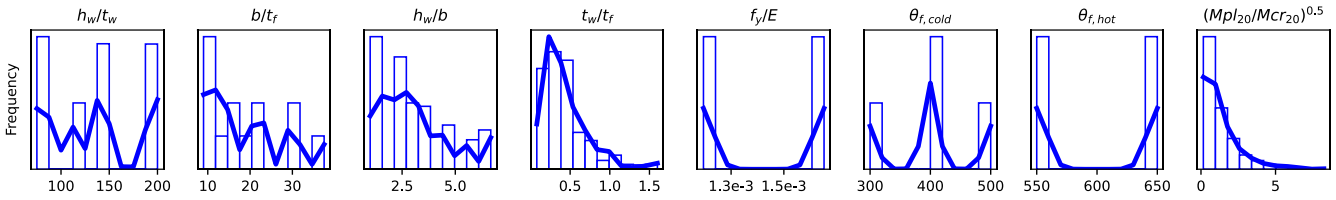

Figure 4. Frequency distribution for the different features.

5 MACHINE LEARNING MODELS

Four different machine learning models were considered in this study, namely Artificial neural networks (ANN), Support vector regression (SVR), Random forests (RF) and Polynomial regression (PR). These models were chosen based on previous experience in their application to regression problems of thin-walled sections in fire [1–3].

The ANN models were implemented using the *pyrenn* [17], which relies on the mean squared error as the loss function and the Levenberg-Marquardt as the optimization algorithm. Among the different architectures, with one or two hidden layers, that were tested, the best performing one was the 8×64×4×1 corresponding to two hidden layers with 64 and 4 neurons.

To train and develop the SVR and RF models, *scikit-learn* library [18] was used. A grid search technique was applied to tune the hyperparameters. Table 2 and Table 3 highlight the hyperparameters that were considered for SVR and RF, respectively, marking with (*) the best ones.

Table 2. Table of hyperparameters used in the SVR [18] (* indicates the best).

kernel	degree	gamma	C	epsilon
Rbf*	1*, 3,	scale, auto	1,	0.1, 0.05
	5, 10,	0.049*, 0.1, 0.0049	10*,	0.01, 0.005*
	100, 1000	0.001, 0.00049	100,	0.0001
			1000	

Table 3. Table of hyperparameters used in the random forests [18] (* indicates the best).

n_estimators	max_depth	min_samples_split	max_features	max_leaf_nodes
10,20,	10, 50,	2 *, 8,	auto*	none*
50, 100,	100*, 500,	16, 24,	log2	10
250, 500,	1000	32, 64	sqrt	100
1000*				500

Finally, the same library was also used to train and develop the PR model. In this case, since models with higher degrees may closely fit most of the data in the training dataset, but possibly at the cost of over-fitting resulting in a larger error on the testing dataset, ridge regression was applied to fit the polynomial feature matrix. We found that a degree 5 polynomial is capable of predicting the resistance of beams within the range of features provided in Table 1 of the numerical dataset.

6 RESULTS AND DISCUSSION

In this section the performance of both analytical and machine learning models is evaluated using different metrics, namely the coefficient of determination R^2, the mean absolute error (MAE) and the mean squared error (MSE). The R^2 measures how well the observations are replicated by a model and a R^2 close to 1 is preferred. The mean absolute error (MAE) quantifies the average magnitude of errors between predicted and actual values, providing a measure of the model's accuracy. On the other hand, the mean squared error (MSE) calculates the average squared differences between predicted and actual values, emphasizing larger

errors due to squaring. It is particularly sensitive to outliers and deviations from the predicted values. While both MAE and MSE provide insights into the model's performance, they offer different perspectives on the accuracy and precision of the predictions, and a lower value is preferred. For the sake of this comparison, the actual and predicted values are considered in terms of the ultimate capacity of the beam $M_{\text{ult,fi}}$. Predictions from the shell FE models are considered as ground truth; validation is available in Refs [19,20].

Figure 5 plots the graphical representation of the accuracy obtained with the ML models, for both the training and testing sets. Values of R^2 are given in the figure. The MAE and MSE are given in Table 4.

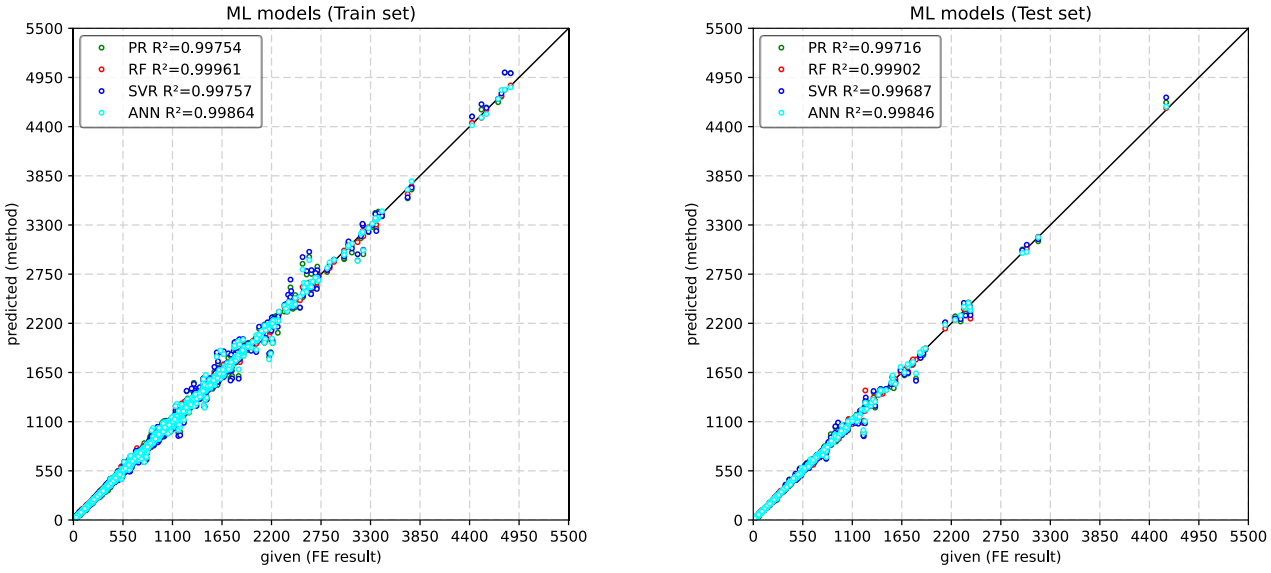

a) b)

Figure 5. Graphical representation of the accuracy obtained with the machine learning models for the a) training and b) testing sets (see Table 4 for MAE and MSE). Values are for ultimate capacity in kN.m.

Table 4. Results of different evaluation metrics for the training and testing sets of ML models.

Model	Set	R^2 [-]	MAE [kN·m]	MSE [(kN·m)^2]
ANN	Train	0.99864	5.63021	18.16122
	Test	0.99846	7.05563	20.25923
SVR	Train	0.99757	8.80275	24.24885
	Test	0.99687	11.29989	28.89603
RF	Train	0.99961	4.30033	9.72442
	Test	0.99902	6.03555	16.18913
PR	Train	0.99754	10.19526	24.39320
	Test	0.99716	12.21141	27.52662

The results show that all the models have good accuracy and are able to predict the capacity of the thin-walled beams under thermal gradients. The best-performing models are the ANN with R^2 of 0.99864 and 0.99846 for training and testing sets, respectively, and RF with R^2 of 0.99961 and 0.99902. In terms of MAE and MSE these are also the models with lowest values. However, it is noticeable that in the ANN the MAE and MSE are more consistent between training and testing sets, with an increase of 7.05563/5.63021≈1.25 and 1.11, while the RF holds 1.40 and 1.66, for MAE and MSE, respectively. A further inspection based on the domain knowledge was carried out using a representation in terms of buckling curves, by plotting the capacity $M_{\text{ult,fi}}$ as a function of a slenderness parameter $\left(M_{pl,20}/M_{cr,20}\right)^{0.5}$. The latter was considered as a feature of the dataset. Note that because of thermal gradients it is simpler to

represent the slenderness parameter at normal temperature. Figure 6 plots the results for beams with two different sections.

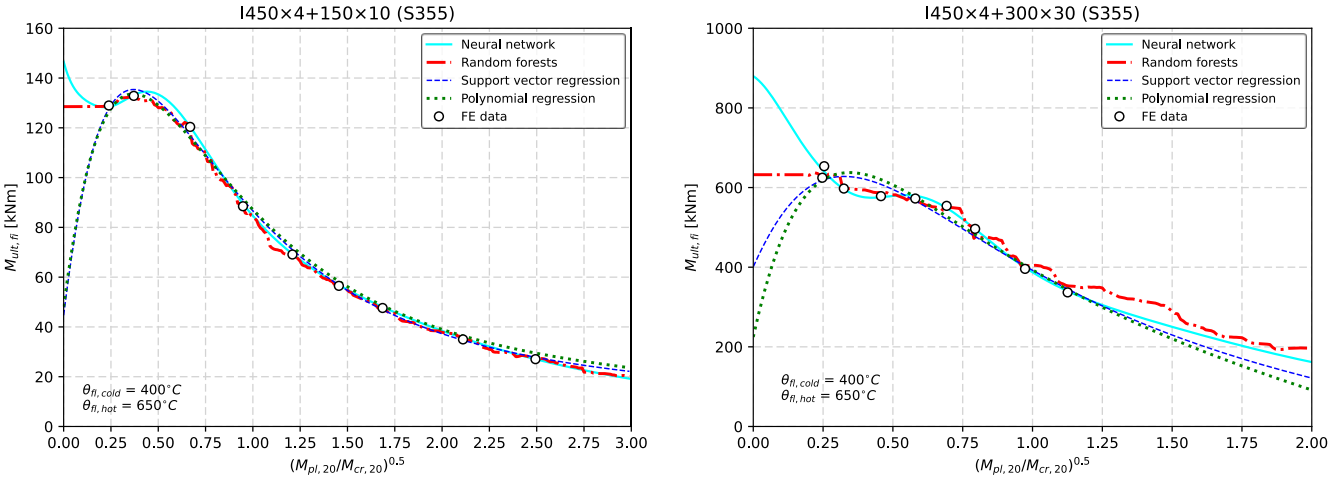

a) b)

Figure 6. Buckling curve representation of the prediction models based on machine learning models for beams with a) I450×4+150×10 and b) I450×4+300×30 sections.

The RF despite being the model with better results in terms of metrics denotes problems when the buckling curve representation is considered. Indeed, we see that the RF model exhibits some jumps/odd behaviour (e.g. at slenderness of 1.0) which is not physically meaningful. In particular, for the I450×4+300×30 beam (Figure 6 b)) we observe that for longer spans the model is diverging. This observation is likely linked with the increase in MAE and MSE that was observed in the results provided in Table 4. On the other hand, the ANN for smaller slenderness values is also overpredicting the beam capacity. The reason for this is related to missing values in the dataset for slenderness below 0.16 (see feature x_8 in Table 1), which can be addressed by increasing the dataset to cover smaller ranges of slenderness. Notwithstanding, the ANN are deemed adequate to be used within the feature range provided in Table 1.

For the analytical models described in section 2, different assumptions were considered in order to compare the results with those obtained numerically and predicted by the machine learning models. Because these analytical models assume a uniform temperature across the section and member length, two extreme cases were considered with a constant temperature equal to the hot flange ($\theta_{fl,hot}$) and cold flange ($\theta_{fl,cold}$). Figure 7 plots the accuracy obtained for these results (for MAE and MSE metrics, see Table 5).

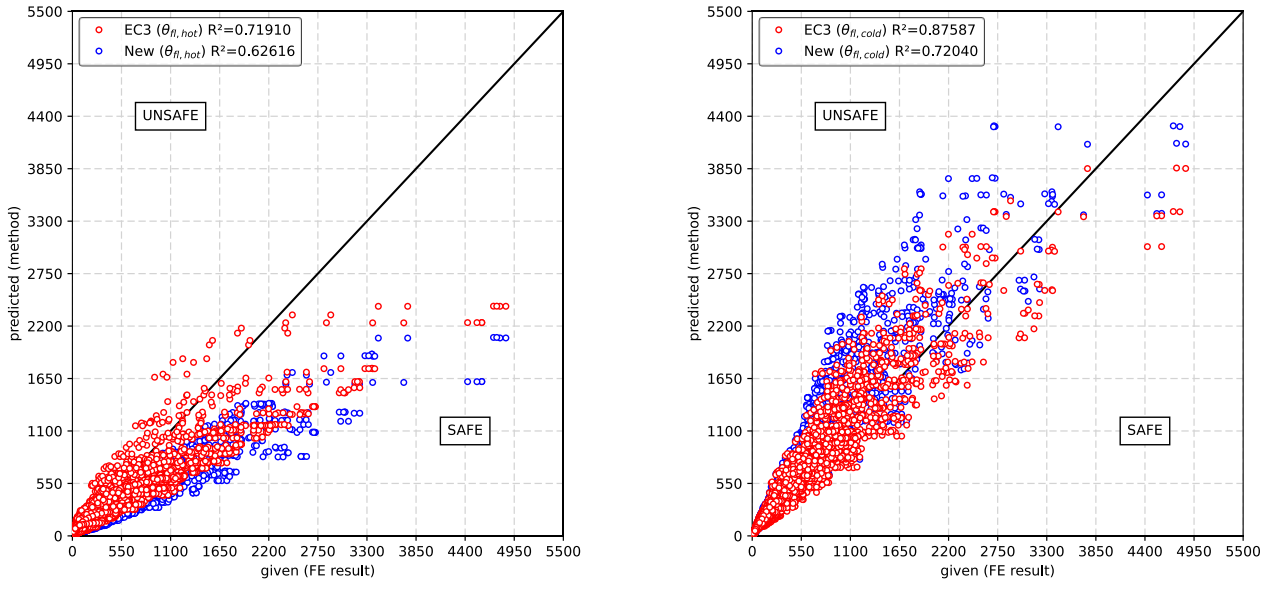

a) Using $\theta_{f,hot}$ in Eq. (6) b) Using $\theta_{f,cold}$ in Eq. (6)

Figure 7. Accuracy obtained with the analytical methods assuming uniform temperature distribution based on either flange.

As expected, both models (EC3 and New generation) fail to adequately predict the beam capacity. The New generation model, with the safe assumption of considering the highest temperature $\theta_{fl,hot}$ everywhere in the section, results in a safe-sided approach but too uneconomical with a R^2 of 0.63.

To test if the lateral-torsional buckling analytical models can predict the beam capacity under thermal gradients, a third assumption was considered where $M_{\text{fi,Rd}}$ and $M_{\text{cr,fi}}$ are numerically determined from the FE analysis. In this latter approach, it is not possible to assess the limits of ESF to choose the correct buckling curve (L1, L2 or L3) thus the least severe one (L3) was considered for the sake of this comparison. Figure 8 plots the results obtained and Table 5 give the metrics for all the model and assumptions regarding the consideration of the analytical models.

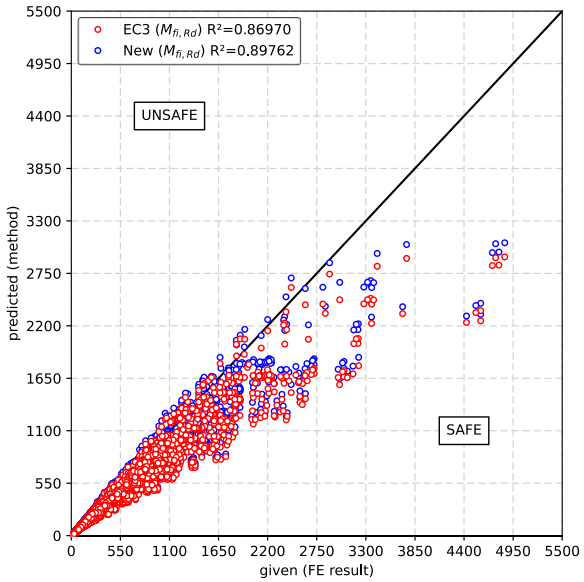

Figure 8. Accuracy obtained with the analytical methods with section resistance and elastic critical moment obtained numerically (note: New generation with curve L3).

Table 5. Results of the accuracy of analytical methods with different assumptions.

Model	Assumption	R^2 [-]	MAE [kN·m]	MSE [(kN·m)²]
EN1993-1-2	Uniform temperature equal to $\theta_{fl,cold}$	0.87587	99.92005	174.26332
	Uniform temperature equal to $\theta_{fl,hot}$	0.71910	144.11253	262.14421
	$M_{\text{fi,Rd}}$ and $M_{\text{cr,fi}}$ from FEA (numeric)	0.86970	77.24774	178.54238
New generation	Uniform temperature equal to $\theta_{fl,cold}$	0.72040	145.37009	261.54127
	Uniform temperature equal to $\theta_{fl,hot}$	0.62616	174.10493	302.42116
	$M_{\text{fi,Rd}}$ and $M_{\text{cr,fi}}$ from FEA (numeric) & L3	0.89762	63.01273	158.26233

The results show that accuracy increases, with R^2 of 0.89762 and 0.86970 obtained for the New generation and EN 1993-1-2 models. This suggests that analytical approaches aiming to increase the accuracy of the section capacity prediction, as well as the elastic critical moment, when thermal gradients are present can be used with the analytical models for the lateral-torsional buckling resistance. In addition, for a more economical model, it might be necessary to further calibrate the lateral-torsional buckling model. For the sake of comparison, Figure 9 plots the results of the analytical models for the different assumptions considered in the form of buckling curves.

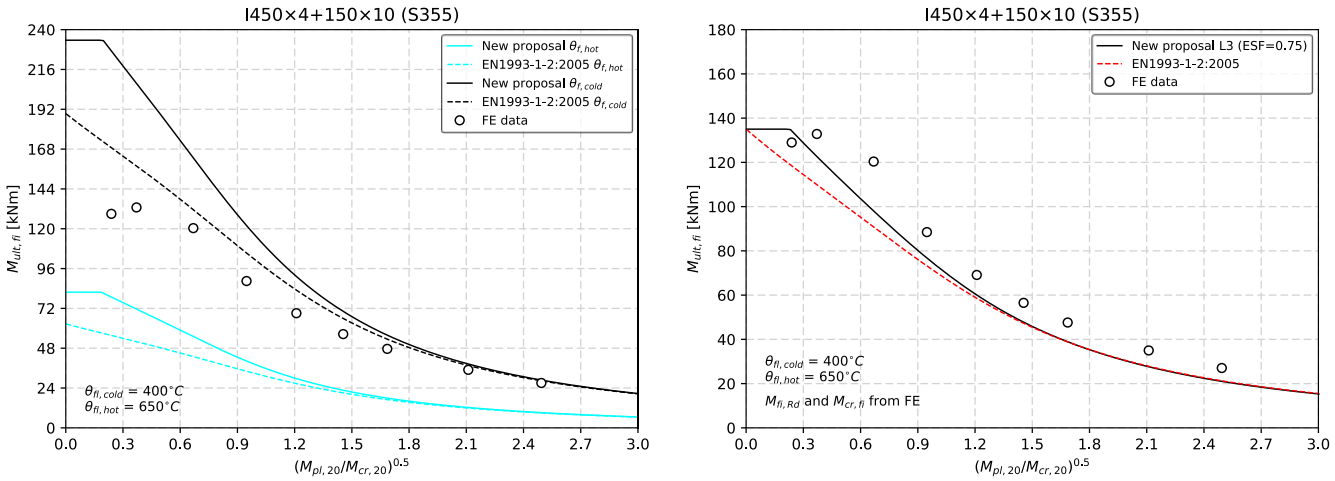

a) b)

Figure 9. Buckling curve representation of the analytical models based on a) uniform temperature of either $\theta_{fl,hot}$ or $\theta_{fl,cold}$ and b) section resistance and elastic critical moment obtained numerically.

7 CONCLUSIONS

As predicting the ultimate strength of laterally unrestrained slender steel beams subjected to fire on three sides remains an elusive problem, we have adopted here Machine Learning (ML) models to investigate the ability to capture the key features and predict the behaviour influenced by local buckling, lateral torsional buckling, and thermal gradients. The key findings are summarized hereafter.

A numerical thermal analysis performed to investigate the thermal gradients that develop in beams heated on three sides found that, when no slab is present, the gradient between the flanges typically ranges between 150 °C and 250°C. The temperature of the web is similar to that in the exposed flange. These results were obtained on a range of protected steel profiles under ISO 834 fire. When a slab is present, lateral-torsional buckling may be prevented but the thermal gradients may reach values higher than 250°C in very slender profiles, which warrants further studies for such conditions.

For the mechanical resistance, a numerical study based on validated nonlinear shell FEM was conducted to build a dataset of 6348 data points for beams with a range of cross-sections, member length, temperatures, and yield strength. The dataset was used to train and test ML models to predict the elevated temperature capacity of the beams. Four ML models were applied to the beam, namely based on artificial neural network (ANN), support vector regression (SVR), random forests (RF) and polynomial regression (PR).

The ML models can fit the results of the shell FE models more closely than the state-of-the-art analytical methods to be included in the next generation of the Eurocodes. For columns, the ML models can predict the resistance at elevated temperature, for both the training and testing dataset, with a R^2 greater than 0.990 for all the models. Further inspection based on domain knowledge and buckling curve representation shows, however, that these models might overpredict the capacity for slenderness ranges outside the training range. These observations also demonstrate that domain knowledge is fundamental to investigate the accuracy of ML models in addition to the usual metrics that are used.

For the analytical models, different assumptions were considered to enable the comparison with the FE results and ML model's prediction. However, these models were not found capable of delivering accurate and economical methodologies despite different simplifying assumptions. One possibility is to develop improved section capacity prediction models when thermal gradients are present, but it might be necessary still to adjust the lateral-torsional buckling models to deliver more economic methodologies.

This work shows that ML models can accurately predict the resistance of beams under non-uniform heating while also being computationally efficient. In future works, beams with higher thermal gradients and with restrained lateral-torsional buckling will be investigated to study cases where a slab is present, as well as beams under different loading conditions.

ACKNOWLEDGMENT

Carlos Couto acknowledges the funding from FCT – Fundação para a Ciência e a Tecnologia, I.P., under the Scientific Employment Stimulus – Institutional Call – CEECINST/00026/2018, and Rede Nacional de Computação Avançada, within the scope of the exploratory research project 2022.15930.CPCA.A1.

Under a license agreement between Gesval S.A. and the Johns Hopkins University, Dr. Gernay and the University are entitled to royalty distributions related to the technology SAFIR described in the study discussed in this publication. This arrangement has been reviewed and approved by the Johns Hopkins University in accordance with its conflict of interest policies.

REFERENCES

1. Couto, C, Tong, Q, Gernay, T: Predicting the capacity of thin-walled beams at elevated temperature with machine learning. Fire Saf J (2022). doi:10.1016/j.firesaf.2022.103596.
2. Couto, C, Tong, Q, Gernay, T: Comparing analytical and machine-learning-based design methods for slender section steel members in fire. 12th Int. Conf. Struct. Fire, Hong Kong (2022)
3. Tong, Q, Couto, C, Gernay, T: Applying Machine Learning to Evaluate the Performance of Thin-Walled Steel Members in Fire, 363–84 (2024). doi:10.1007/978-3-031-48161-1_15.
4. Wong, MB: Adaptation factor for moment capacity calculation of steel beams subject to temperature gradient. J Constr Steel Res 63:1009–15 (2007). doi:10.1016/j.jcsr.2006.10.004.
5. Li, G, Wang, P, Shouchao, J: Non-linear finite element analysis of axially restrained steel beams at elevated temperatures in a fire. J Constr Steel Res 63:1175–83 (2007). doi:10.1016/j.jcsr.2006.11.009.
6. Pi, Y-L, Bradford, MA: Thermoelastic lateral-torsional buckling of fixed slender beams under linear temperature gradient. Int J Mech Sci 50:1183–93 (2008). doi:10.1016/j.ijmecsci.2008.04.004.
7. Ragheb, WF: Local buckling capacity of steel I-section beams subjected to uniform or linear temperature gradient. Thin-Walled Struct 119:304–14 (2017). doi:10.1016/j.tws.2017.06.017.
8. CEN: EN 1993-1-2, Eurocode 3: Design of steel structures - Part 1-2: General rules - Structural fire design (2005).
9. CEN: FprEN 1993-1-2, Eurocode 3: Design of steel structures - Part 1-2: General rules - Structural fire design (2023).
10. CEN: EN 1993-1-5, Eurocode 3 - Design of steel structures - Part 1-5: Plated structural elements (2006).
11. Couto, C, Vila Real, P, Lopes, N, Zhao, B: Resistance of steel cross-sections with local buckling at elevated temperatures. J Constr Steel Res 109:101–14 (2015). doi:10.1016/j.jcsr.2015.03.005.
12. Couto, C, Vila Real, P, Lopes, N, Zhao, B: Numerical investigation of the lateral–torsional buckling of beams with slender cross sections for the case of fire. Eng Struct 106 (2016). doi:10.1016/j.engstruct.2015.10.045.
13. Franssen, J-M, Gernay, T: Modeling structures in fire with SAFIR®: theoretical background and capabilities. J Struct Fire Eng 8:300–23 (2017). doi:10.1108/JSFE-07-2016-0010.
14. Couto, C, Vila Real, P: The influence of imperfections in the critical temperature of I-section steel members. J Constr Steel Res 179 (2021). doi:10.1016/j.jcsr.2021.106540.
15. ANSYS®. Academic Research Mechanical, Release 18.2 2018.
16. Couto, C, Vila Real, P, Lopes, N, Zhao, B: Numerical investigation of the lateral torsional buckling of beams with slender cross-sections for the case of fire. Eng Struct 106:410–21 (2016).
17. Atabay, D: pyrenn: A recurrent neural network toolbox for Python and Matlab. Inst Energy Econ Appl Technol Tech Univ München, Http//Pyrenn Readthedocs Io/En/Latest (2024).
18. Pedregosa, F, Varoquaux, G, Gramfort, A, Michel, V, Thirion, B, Grisel, O, et al: Scikit-learn: Machine learning in Python. J Mach Learn Res 12:2825–30 (2011).
19. Prachař, M, Lopes, N, Couto, C, Jandera, M, Vila Real, P, Wald, F: Lateral torsional buckling of Class 4 Steel Plate Girders Under Fire Conditions: Experimental and Numerical Comparison. In: Wald F., Burgess I., Kwasniewski L., Horová K. CE, editor. Benchmark Stud. - Exp. Valid. Numer. Model. fire Eng., CTU Publishing House, Czech Technical University in Prague 21–33 (2011).
20. FIDESC4: Fire Design of Steel Members with Welded or Hot-Rolled Class 4 Cross-Section, RFCS-CT-2011-00030, (2014).